

# Exploiting the crossterms of the virtual Rayleigh-wave Green tensor for surface-wave inversion

*K. van Wijk\**, Department of Geosciences, Boise State University

*H. Douma*, ION Geophysical/ GXT Imaging Solutions

*D. Mikesell and M. Haney*, Department of Geosciences, Boise State University

## SUMMARY

Surface-wave tomography from the correlations of ambient noise records has provided a powerful tool to investigate the Earth's subsurface with new surface-wave information. Exploration surveys can benefit from inversion of these virtual surface waves, as well. Most commonly, correlations are performed on the vertical components of the wavefields, but here we use the crossterms of multicomponent data and show virtual surface wave recordings are less sensitive to artifacts from signal not in-line with the two stations. We illustrate this with a subsection of the Coronation data set and the Batholiths temporary seismic deployment, showing estimates of the Rayleigh wave and the consequent phase-velocity dispersion curve.

## INTRODUCTION

Being able to estimate the impulse response between seismic stations from crosscorrelating noise wavefields has added a new dimension to surface-wave inversion for the Earth's lithosphere. Phase- and group-velocity dispersion curves between distributed station pairs are inverted for 3D velocity structure (e.g., Sabra et al., 2005; Shapiro et al., 2005; Lin et al., 2008; Ekstrom et al., 2009). Ideally, station pairs are surrounded by ambient seismic noise sources (mostly thought to be associated with the oceans). The exploration seismology community is benefiting from parallel developments by inverting surface waves for near-surface structure (Haney and Douma, 2010; Gouedard et al., 2011). Here we aim to optimize surface-wave information via seismic interferometry on combinations of the vertical and radial components of the wavefield.

The elastic Green tensor can then be found by summing cross-correlations of the different components ( $i, j$ ) of the wavefield (Wapenaar and Fokkema, 2006):

$$G_{ij}(\mathbf{x}, \mathbf{x}', t) + G_{ij}(\mathbf{x}, \mathbf{x}', -t) \propto \oint_S u_i^S(\mathbf{x}, t) \star u_j^S(\mathbf{x}', t) d\mathbf{S}, \quad (1)$$

where  $G_{ij}(\mathbf{x}, \mathbf{x}', t)$  is the Green tensor with component  $j$  at location  $\mathbf{x}$  from a source in direction  $i$  at  $\mathbf{x}'$ .  $u_i^S(\mathbf{x}, t)$  and  $u_j^S(\mathbf{x}', t)$  are the components of the measured wavefield at  $\mathbf{x}$  and  $\mathbf{x}'$  from a source on contour  $S$ . The  $\star$  indicates the crosscorrelation operator.

A vertically heterogeneous earth has an anti-symmetry between the horizontal component of the Rayleigh wave from a vertical force source, and the vertical component of the Rayleigh wave from a horizontal force source (equation 7.147 of Aki and Richards, 1980):

$$G_{rz}(\mathbf{x}, \mathbf{x}', t) = -G_{rz}(\mathbf{x}', \mathbf{x}, t) = -G_{zr}(\mathbf{x}, \mathbf{x}', t), \quad (2)$$

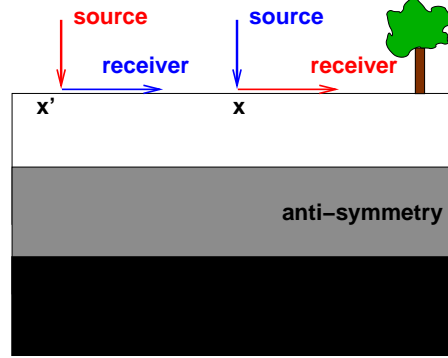


Figure 1: The antisymmetry of the crossterms of the Rayleigh-wave Green tensor can be seen from the receiver for the blue experiment pointing inward, while the red receiver is pointing away from its source. This means these wavefields are of opposite sign.

where subscript  $r$  stands for radial and  $z$  for vertical. For a retrograde elliptical Rayleigh wave,  $G_{rz}$  is 90 degrees phase-delayed with respect to  $G_{zz}$  and a 180 degrees phase-delayed with respect to  $G_{zr}$ . In graphical form, the antisymmetry is displayed in Figure 1.

After obtaining estimates of the Rayleigh-wave Green tensor via equation 1, we compare  $G_{zz}$  to  $G_{zr} - G_{rz}$ . The Hilbert transform (e.g., page 20 of Claerbout, 1985) equalizes the phase between  $G_{zz}$  and the difference of the cross terms:

$$G_c(\mathbf{x}, \mathbf{x}', t) = \mathcal{H} [G_{zr}(\mathbf{x}, \mathbf{x}', t) - G_{rz}(\mathbf{x}, \mathbf{x}', t)]. \quad (3)$$

Crosscorrelations of multicomponent data from the Coronation data set illustrate the value of using these crossterms. In addition, the Batholiths passive seismic experiment (Calkins et al., 2010) provides estimates of the crossterms of the Green tensor  $G_c$  that are more robust than  $G_{zz}$  in the presence of seismic signal not in-line with the stations.

## CORONATION DATA

Figure 2 is a map of sources and receivers for a subset of the 80 km<sup>2</sup> Coronation field data set, where sources are 1 kg of dynamite buried at 18 m and the receivers are three components (Calvert et al., 2005). The horizontal receivers are oriented such that there is an East-West (radial) and a North-South (transverse) component. Surface-wave inversion between (virtual) source-receiver pairs can be used for near-surface characterization (Haney and Douma, 2010; Gouedard et al., 2011). In the following we present robust virtual source-receiver pairs with the aim to increase resolution in velocity models from surface-wave inversion.

## Exploiting the Crossterms of Rayleigh Waves

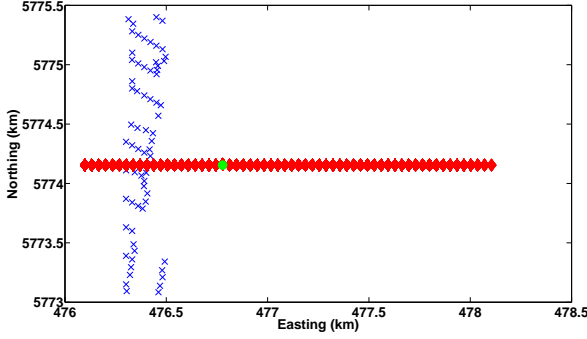


Figure 2: A map of the subset of sources and receivers of the Coronation data set. Blue symbols are sources, and red diamonds are receivers. The green symbol is the location of the virtual source used in this abstract.

The top panel in Figure 3 is the virtual shot record from 1-5 Hz obtained from seismic interferometry applied to the vertical component data. The bottom panel is the difference between the crossterms of the Green tensor estimated via seismic interferometry.

The tenth receiver in the shotrecords is depicted in Figure 4 to emphasize key differences between  $G_{zz}$  and  $G_c$ : the latter result lacks the strong artifact near  $t = 0$ , and the Rayleigh wave has a larger signal-to-noise ratio than  $G_{zz}$ . For more insight into the crossterms, Figure 5 shows the antisymmetry of these crossterms. Amplitudes of the two crossterms are not equal. This may be due to a violation of the lateral homogeneity under the virtual source-receiver pair, or a difference in coupling between stations. Nevertheless, the difference of these terms clearly benefits from constructive interference.

We have shown that we can use a subset of the sources to increase the number of (virtual) source-receiver pairs that can go into a surface-wave inversion scheme via seismic interferometry. This number may be further grown by obtaining the Green tensor between sources, appealing to reciprocity (Curtis et al., 2009). Ultimately, the goal is to improve resolution in the surface-wave inversion scheme. The next section is one step closer to this goal, as we illustrate a more coherent dispersion curve for the crossterm results.

### BATHOLITHS DATA

In passive seismic interferometry, the spatial integration in equation 1 is replaced with summation over  $k$  time sections of the wavefield  $u$ , aiming to capture surface-wave signal from sources around the stations at  $(\mathbf{x}, \mathbf{x}')$ :

$$G_{ij}(\mathbf{x}, \mathbf{x}', t) \approx \sum_k (u_j(\mathbf{x}', t) \star u_i(\mathbf{x}, t))_k. \quad (4)$$

Vertical component ( $i = j = z$ ) Rayleigh wave estimates are most commonly used in ambient noise tomography, but an uneven source distribution and contamination by wave modes other than Rayleigh waves can lead to artifacts in the estimated

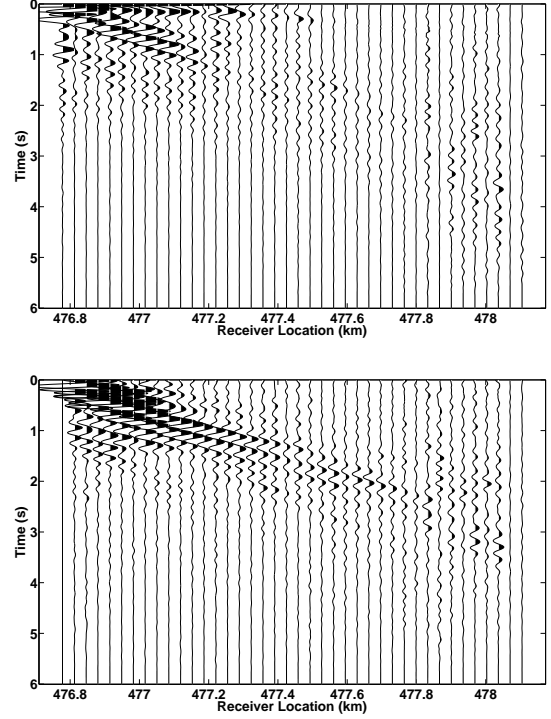


Figure 3: Estimated Green functions for  $G_{zz}$  (top) and  $G_c$  (bottom). For the smaller station spacings in  $G_{zz}$ , an artifact is present at  $t \approx 0$  s.  $G_c$  lacks most of this artifact, and appears more coherent at greater offsets.

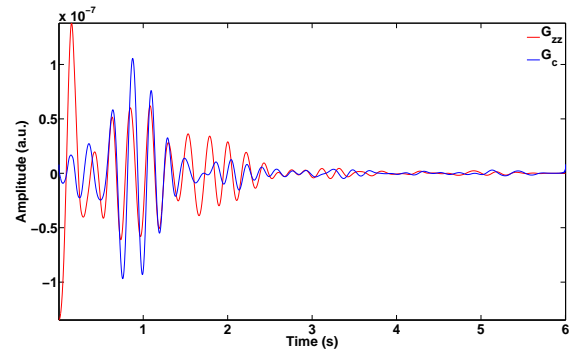


Figure 4: A comparison between  $G_{zz}$  (red) and  $G_c$  (blue) for the receiver 10 stations East of the virtual source.

## Exploiting the Crossterms of Rayleigh Waves

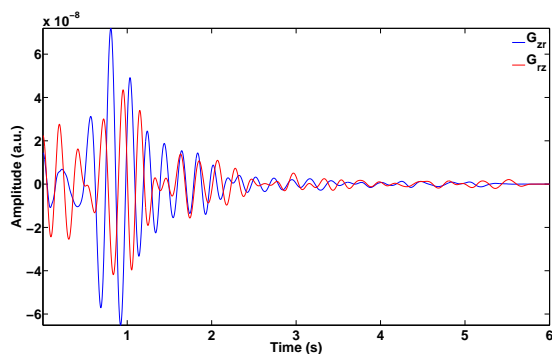


Figure 5: A comparison between  $G_{zr}$  (blue) and  $G_{rz}$  (red) for the receiver 10 stations to the East of the virtual source.

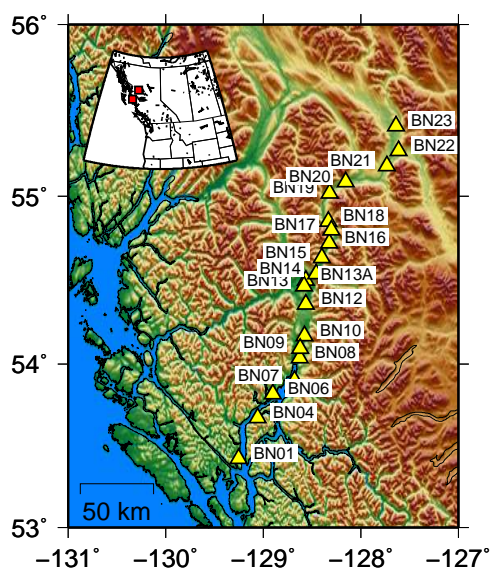


Figure 6: Map of the active stations in August 2006 of the North line of the Batholiths experiment. Red squares on the regional inset are BN01 and BN23.

Green functions from cross correlation. Wapenaar et al. (2011) show in a numerical example how multi-dimensional deconvolution can suppress unwanted signal, but we propose to exploit the crossterms of the Green tensor estimated from crosscorrelation (van Wijk et al., 2011).

The azimuth from station BN01 to BN23 from the north line of the Batholiths experiment is 29 degrees from North in the clockwise direction (Figure 6). We rotate the horizontal components of the wavefield recordings to a generally radial ( $r$ ) and transverse ( $t$ ) component, band-pass filter (0.1 - 1 Hz), and sign-bit the data. We then crosscorrelate combinations of the vertical and radial components of the wavefield from station BN01 with those of all 20 active stations according to equation 4. The Green tensor estimate is the sum of non-overlapping, ten-minute crosscorrelations from August 1, 2006 00:00:00 (HH:MM:SS) to August 4, 2006 00:00:00. We correct the amplitudes for geometrical spreading.

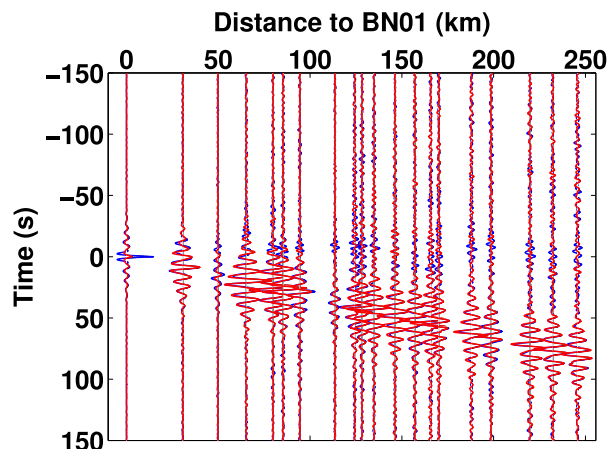


Figure 7: Estimated Green functions for  $G_{zz}$  (blue) and  $G_c$  (red). For the smaller station spacings in  $G_{zz}$ , an artifact at  $t \approx 0$  s interferes with the Rayleigh wave.

van Wijk et al. (2011) show a dominant source area to the West, with a secondary region to the Southwest, both with slownesses typical for Rayleigh waves. The dominant energy from the West propagates obliquely to the array, and is the source for the out-of-line energy observed close to zero lag time in the vertical component (blue) crosscorrelations in Figure 7. The crossterm combination  $G_c$  (red) is also shown in Figure 7. The  $G_c$  estimates lack the artifact near zero time lag attributed to out-of-line sources to the West. Biased velocity and/or amplitude information in the estimate of the Rayleigh wave could be erroneously attributed to attenuation and anisotropy (also discussed in Harmon et al., 2010).

To illustrate the improvement of  $G_c$  compared to  $G_z$ , we compute the phase-velocity dispersion curve – commonly used to invert for velocity structure. We compute phase-velocity dispersion curves using the Full-Offset Dispersion Imaging technique (Park, 2011), which includes spectral whitening in the phase-velocity transformation. Figure 8 shows more coherence in  $G_c$  than the dispersion curve obtained from  $G_{zz}$ .

## FUTURE WORK: SPAC

An alternative way to obtain surface wave dispersion information is the spatial autocorrelation method (SPAC), where the spatial distribution of the crosscorrelated wavefields are fit by Bessel functions, dependent on the velocity as a function of frequency (Aki, 1957). (Haney et al., 2011) show that our results for the off-diagonal components of the Rayleigh wave correlation coefficient matrices, combined with Aki's results

## Exploiting the Crossterms of Rayleigh Waves

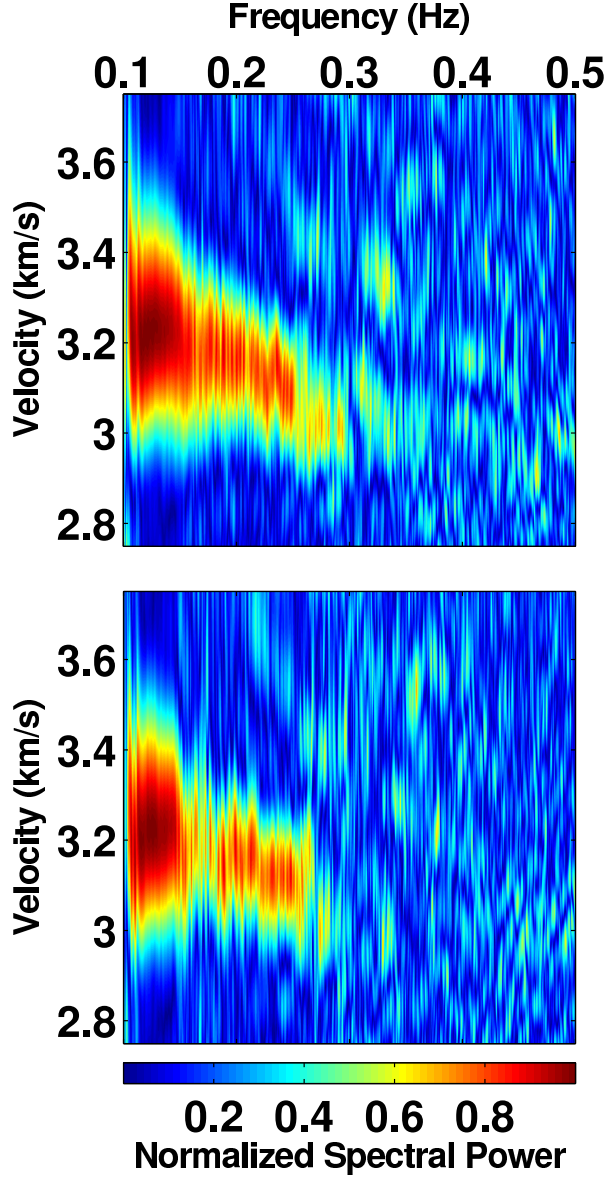


Figure 8: Phase velocity dispersion curve for the estimated Rayleigh-wave Green function. The dispersion curve for the cross terms  $G_c$  (top) has greater coherence across the spectrum than the result for the vertical component of the wavefield  $G_{zz}$  (bottom).

for the main diagonal, can be summarized as follows:

$$\phi^R(r, \omega) = \begin{bmatrix} \phi_{ZZ}^R & \phi_{ZR}^R & \phi_{ZT}^R \\ \phi_{RZ}^R & \phi_{RR}^R & \phi_{RT}^R \\ \phi_{TZ}^R & \phi_{TR}^R & \phi_{TT}^R \end{bmatrix} = P^R(\omega) \times \begin{bmatrix} J_0(\frac{\omega r}{c_R}) & -R J_1(\frac{\omega r}{c_R}) & 0 \\ R J_1(\frac{\omega r}{c_R}) & \frac{R^2}{2} [J_0(\frac{\omega r}{c_R}) - J_2(\frac{\omega r}{c_R})] & 0 \\ 0 & 0 & \frac{R^2}{2} [J_0(\frac{\omega r}{c_R}) + J_2(\frac{\omega r}{c_R})] \end{bmatrix} \quad (5)$$

For completeness, here is the result for Love waves:

$$\phi^L(r, \omega) = \begin{bmatrix} \phi_{ZZ}^L & \phi_{ZR}^L & \phi_{ZT}^L \\ \phi_{RZ}^L & \phi_{RR}^L & \phi_{RT}^L \\ \phi_{TZ}^L & \phi_{TR}^L & \phi_{TT}^L \end{bmatrix} = P^L(\omega) \times \begin{bmatrix} 0 & 0 & 0 \\ 0 & \frac{1}{2} [J_0(\frac{\omega r}{c_L}) + J_2(\frac{\omega r}{c_L})] & 0 \\ 0 & 0 & \frac{1}{2} [J_0(\frac{\omega r}{c_L}) - J_2(\frac{\omega r}{c_L})] \end{bmatrix}, \quad (6)$$

where  $\omega$  is angular frequency,  $r$  is radial distance,  $c_R$  is Rayleigh wave velocity,  $c_L$  is Love wave velocity,  $R$  is the ratio of the horizontal-to-vertical motion of the Rayleigh waves,  $P^R$  is the power spectrum of the Rayleigh waves,  $P^L$  is the power spectrum of the Love waves, and  $J_0$ ,  $J_1$ , and  $J_2$  are Bessel functions of the zeroth, first, and second orders, respectively.

## CONCLUSIONS

Correlations of multicomponent wavefields from the Corona-tion seismic experiment provide estimates of the Rayleigh-wave Green tensor. These estimates can serve in surface-wave inversion for near-surface velocity models. Taking advantage of anti-symmetry, the difference between the crossterms provides a superior estimate compared to the estimate from cross-correlations of the vertical components only. The crossterm result is especially robust in the presence of out-of-line Rayleigh waves. Improvements in signal-to-noise ratio and suppression of artifacts in the estimated Rayleigh waves allow us to include more (virtual) source-receiver pairs in surface-wave inversion for velocity models of the near surface.

## ACKNOWLEDGMENTS

We thank Vera Schulte-Pelkum and Joshua Stachnik for the work on the Batholiths data set.

## Exploiting the Crossterms of Rayleigh Waves

### REFERENCES

- Aki, K., 1957, Space and time spectra of stationary stochastic waves, with special reference to microtremors: *Bulletin of Earthquake Research Institute*, **35**, 415–457.
- Aki, K., and P. G. Richards, 1980, *Quantitative seismology: theory and practice*: Freeman.
- Calkins, J. A., G. Zandt, J. Girardi, K. Dueker, G. E. Gehrels, and M. N. Ducea, 2010, Characterization of the crust of the Coast Mountains Batholith, British Columbia, from P to S converted seismic waves and petrologic modeling: *Earth and Planetary Science Letters*, **289**, 145 – 155.
- Calvert, A. S., J. M. Novak, J. Maher, D. N. Burch, D. Bird, and R. Larson, 2005, A tale of two surveys: experiences processing two similar but different land 3d-3c mems surveys: *SEG Technical Program Expanded Abstracts*, **24**, 975–978.
- Claerbout, J. F., 1985, *Fundamentals of geophysical data processing*: Blackwell Scientific.
- Curtis, A., H. Nicolson, D. Halliday, J. Trampert, and B. Baptie, 2009, Virtual seismometers in the subsurface of the earth from seismic interferometry: *Nature Geoscience*, **2**, 700704. (DOI: 10.1038/NGEO615).
- Ekstrom, G., G. A. Abers, and S. C. Webb, 2009, Determination of surface-wave phase velocities across USArray from noise and Akis spectral formulation: *Geophysical Research Letters*, **36**, L18301. (doi:10.1029/2009GL039131).
- Gouedard, P., P. Roux, M. Campillo, A. Verdel, H. Yao, and R. D. van der Hilst, 2011, Source depopulation potential and surface-wave tomography using a crosscorrelation method in a scattering medium: *Geophysics*, **76**, SA51–SA61.
- Haney, M., D. Mikesell, and K. van Wijk, 2011, Extension of the spatial autocorrelation (SPAC) method to mixed-component correlations of diffuse seismic waves. in preparation.
- Haney, M. M., and H. Douma, 2010, Imaging lateral heterogeneity at coronation field with surface waves: *SEG Technical Program Expanded Abstracts*, **29**, 1851–1855.
- Harmon, N., C. Rychert, and P. Gerstoft, 2010, Distribution of noise sources for seismic interferometry: *Geoph. J. Int.*, **183**, 1470–1484.
- Lin, F., M. P. Moschetti, and M. H. Ritzwoller, 2008, Surface wave tomography of the western United States from ambient seismic noise: Rayleigh and Love wave phase velocity maps: *Geophys. J. Int.*, **173**, 281–298. (doi:10.1111/j1365-1246X.2008.3720.x).
- Park, C. B., 2011, Imaging dispersion of masw data—full vs. selective offset scheme: *Journal of Environmental and Engineering Geophysics*, **16**, 13–23.
- Sabra, K. G., P. Gerstoft, P. Roux, W. A. Kuperman, and M. C. Fehler, 2005, Surface wave tomography from microseisms in Southern California: *Geophysical Research Letters*, **32**, L14311–L14311.
- Shapiro, N. M., M. Campillo, L. Stehly, and M. H. Ritzwoller, 2005, High-resolution surface-wave tomography from ambient seismic noise: *Science*, **307**, 1615–1618.
- van Wijk, K., D. Mikesell, V. Schulte-Pelkum, and J. Stachnic, 2011, Estimating the rayleigh-wave impulse response between seismic stations with the cross terms of the green tensor. Under review.
- Wapenaar, K., and J. Fokkema, 2006, Green’s function representations for seismic interferometry: *Geophysics*, **71**, SI33–SI46.
- Wapenaar, K., E. Ruigrok, J. van der Neut, and D. Draganov, 2011, Improved surface-wave retrieval from ambient seismic noise by multi-dimensional deconvolution: *Geophysical Research Letters*, **38**, L01313.